

Fractal Quasicondensation in One dimension

Flavio Riche,¹ Miguel Gonçalves,¹ Bruno Amorim,² Eduardo V. Castro,^{3,4} and Pedro Ribeiro^{1,4}

¹*CeFEMA, LaPMET, Instituto Superior Técnico,*

Universidade de Lisboa, Av. Rovisco Pais, 1049-001 Lisboa, Portugal

²*Centro de Física das Universidades do Minho e Porto, LaPMET,*

Universidade do Minho, Campus of Gualtar, 4710-057, Braga, Portugal

³*Centro de Física das Universidades do Minho e Porto, LaPMET,*

Departamento de Física e Astronomia, Faculdade de Ciências,

Universidade do Porto, 4169-007 Porto, Portugal

⁴*Beijing Computational Science Research Center, Beijing 100084, China*

We unveil a novel mechanism for quasicondensation of hard-core bosons in the presence of quasiperiodicity-induced multifractal single-particle states. The new critical state, here dubbed fractal quasicondensate, is characterized by natural orbitals with multifractal properties and by an occupancy of the lowest natural orbital, $\lambda_0 \simeq L^\gamma$, which grows with system size but with a non-universal scaling exponent, $\gamma < 1/2$. In contrast to fractal quasicondensates obtained when the chemical potential lies in a region of multifractal single-particle states, placing the chemical potential in regions of localized or delocalized states yields, respectively, no condensation or the usual 1D quasicondensation with $\gamma = 1/2$. Our findings are established by studying one-dimensional hard-core bosons subjected to various quasiperiodic potentials, including the well-known Aubry-André model, employing a mapping to non-interacting fermionics that allows for numerically exact results. We discuss how to test our findings in state-of-the-art ultracold atom experiments.

The localization of single-particle wave functions predicted by Anderson [1] can be induced by uncorrelated disorder or by quasiperiodic (QP) perturbations incommensurate with the underlying crystal. quasiperiodicity can induce localization-delocalization transitions even in one dimension [2], where any finite amount of uncorrelated disorder immediately localizes the wave function [3–6]. QP modulations may also lead to critical states with multifractal properties [7–11]. Such critical states arise at localization phase transitions and were also shown to ensue in extended areas of the phase space, where they can coexist with localized and extended states, albeit separated by the so-called mobility edges into different spectral regions [12–16].

Interest in QP single-particle systems, kickstarted in the 80's by the celebrated Aubry-André (AA) model [2], has been renewed by the possibility of engineering QP modulations in arrays of trapped atoms, cavity polaritons, and photonic lattices [7, 17–22] and by the emergence of moiré systems, such as twisted bilayer graphene [23, 24].

In the presence of interactions, the effects of the interplay between quasiperiodicity and strong interactions is a subject under active investigation [25–27]. For one, it is yet unclear if electron-electron interactions and quasiperiodicity combined can explain the physics of twisted bilayer graphene [23, 28, 29].

In interacting bosonic systems, the Bose condensed state may also be affected by QP modulations [30–33]. Its effects can even be observed in one dimension, where a macroscopic occupation of the condensed state is not possible and, instead, the superfluid phase is characterized by an occupation of the most populated state that grows as the square root of the total number of bosons [34].

This so-called quasicondensed state can be destroyed by a QP perturbation yielding a compressible insulating phase dubbed Bose glass [21, 35–40]. In the strongly-coupling limit, where repulsive on-site interactions render bosons effectively hard-core particles, these effects have been well-established thanks to the Jordan-Wigner (JW) mapping onto non-interacting fermions [41]. As a result, a numerically exact analysis may be conducted for relatively large system sizes [12, 36, 42]. This has permitted to show that, when submitted to a QP potential, hard-core boson (HCB) lattices, host quasicondensed, Mott insulating or Bose glass phases, depending on the location of the chemical potential μ [12]. If μ lies in a spectral region where JW single-particle states are delocalized (localized), the system is a quasicondensate (Bose glass), and the fraction of particles in the most occupied state, λ_0 , behaves as $N_b^{1/2}$ (N_b^0), with N_b the total number of bosons. If μ lies in a spectral gap the system is a Mott insulator with $\lambda_0 \sim N_b^0$.

Here, we investigate the fate of the quasicondensed state when the chemical potential lies within a spectral region of fractal single-particle eigenstates arising at localization-delocalization transitions or in extended phase-space regions [7, 8, 43]. We show that critical 1D HCB are fractal quasicondensates, characterized by fractional occupation $\lambda_0 \sim N_b^\gamma$, with $0 < \gamma < 1/2$, and that the quasicondensed state exhibits multifractal localization properties. In the critical regime, the scaling exponent, γ , was found to be non-universal. To illustrate our findings we consider the AA model at criticality, and the Ganeshan-Pixley-Sarma (GPS) model [8] having anomalous mobility edges. Some of these results are summarized in Fig. 1, where we also show the single-particle inverse participation ratio (IPR) throughout the phase

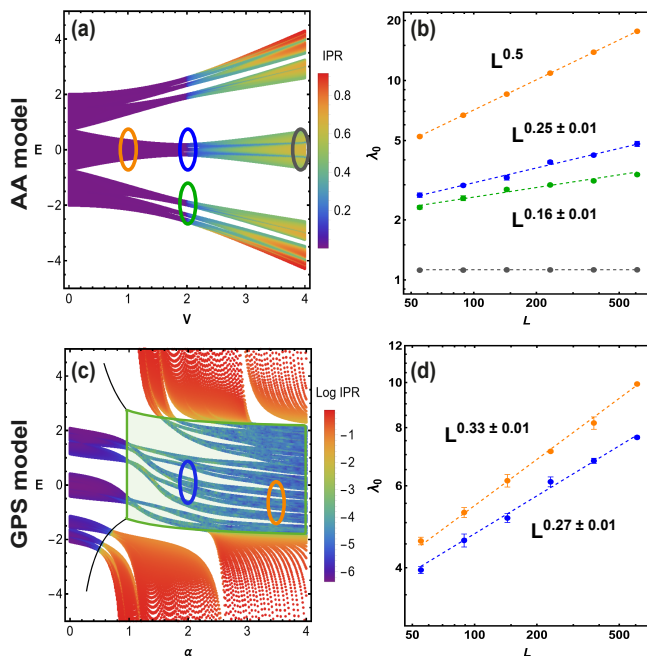


FIG. 1. **AA model.** (a) IPR for the single-particle eigenstates as a function of the quasiperiodic potential strength, V , and energy, E , for system size $L = 610$. (b) Scaling of the natural orbital's highest eigenvalue, λ_0 , as a function of L for delocalized ($V = 1$, orange), critical ($V = 2$, blue), and localized ($V = 4$, gray) states at filling fraction $\nu = 1/2$. We also plot the scaling of critical states for $V = 2$ at $\nu = 0.29$ (green) to show that Bose superfluidity occurs for other filling fractions than $\nu = 1/2$. **GPS model.** (c) IPR as a function of α and E , computed for $V = 0.75$ and $L = 610$. Black curves indicate extended-localized transitions. Critical phase is shaded in green. (d) Scaling of λ_0 with L for $\alpha = 2$ at $\nu = 0.48$ ($\alpha = 3.5$ at $\nu = 0.368$), where blue (orange) points are numerical results fitted by the dashed lines. Fractal quasicondensation is revealed by the sub-linear scalings $\lambda_0 \propto L^\gamma$ with $0 < \gamma < 1/2$. Results in (b,d) are averaged over 10 random configurations of θ and ϕ . Error bars are obtained from the standard deviation of the configurational average.

diagram of the AA and GPS models.

In the remainder of this letter, we present the models and detail our analysis of the occupations and of the properties of the fractal quasicondensed state, we discuss our findings, and how our results may be observed experimentally. Additional data corroborating our conclusions and a discussion on particular implementations are provided as Supplemental Material [44].

Model and Methods.— We consider N_b HCB on a 1D lattice with L sites and periodic boundary conditions. The Hamiltonian is given by:

$$H = - \sum_n (t b_n^\dagger b_{n+1} + \text{h.c.}) + \sum_n V_n^\gamma b_n^\dagger b_n, \quad (1)$$

where b_n (b_n^\dagger) is the bosonic annihilation (creation) operator at site $n = 1, \dots, L$. The hard-core limit imposes

the constraints $b_n^2 = b_n^{\dagger 2} = 0$ and imply the same-site anti-commutation relation, $\{b_n, b_n^\dagger\} = 1$, in addition to the usual commutation relations, $[b_n, b_m^\dagger] = \delta_{n,m}$, for $n \neq m$. t is the hopping integral and V_n^γ is the on-site incommensurate potential specified below (γ labels the two potentials considered). We apply twisted boundary conditions, i.e. $b_n^\dagger = b_{n+L}^\dagger e^{i\theta}$, with phase twists θ , that can be easily implemented through the Peierls substitution, $t \rightarrow t e^{i\theta/L}$. Subsequent numerical results are presented in units of t .

After the JW mapping, $b_n^\dagger = c_n^\dagger \prod_{\beta=1}^{n-1} e^{-i\pi c_\beta^\dagger c_\beta}$, with c_n (c_n^\dagger) the fermionic annihilation (creation) operator, the fermionic Hamiltonian is given by Eq. (1), replacing b_n by c_n . The bosonic single-particle density matrix (SPDM), $\rho_{nm}^B = \langle b_n^\dagger b_n \rangle$, can be efficiently computed from its fermionic counterpart, $\rho_{nm}^F = \langle c_m^\dagger c_n \rangle$, computed by evaluating matrix determinants [34, 41]. Since the form of H remains unchanged after the JW mapping, both HCB and free fermions share the same energy spectrum. For diagonal entries $\rho_{nn}^B = \rho_{nn}^F$, thus differences between fermionic and bosonic single-particle density matrices are encoded in their off-diagonal correlations.

For homogeneous systems at zero temperature, quasicondensation is signaled by a divergence in the momentum distribution function at zero momentum $n_{\kappa=0} \sim \sqrt{N_b}$ [34]. The generalization for spatially inhomogeneous systems amounts to considering the highest eigenvalue of the bosonic SPDM, λ_0 . The eigenvectors of the SPDM, Φ_j^n , are called *natural orbitals* (NO), i.e. [41, 45, 46]:

$$\sum_j \rho_{ij}^B \Phi_j^n = \lambda_n \Phi_i^n, \quad (2)$$

with $\lambda_0 \geq \lambda_1 \geq \dots$. The number of bosons in the most occupied state scales with N_b , $\lambda_0 \sim (N_b)^\gamma$, with $\gamma = 0.5$ for quasicondensates associated with delocalized states and $\gamma = 0$ for Mott insulators and Bose Glasses.

Concerning the QP potential, V_n^γ , the index $\gamma = \text{AA}$, GPS labels the two considered models, with potentials respectively given by:

$$V_n^{\text{AA}} = V \cos(2\pi\tau n + \phi), \quad (3)$$

$$V_n^{\text{GPS}} = \frac{V \cos(2\pi\tau n + \phi)}{1 + \alpha \cos(2\pi\tau n + \phi)}. \quad (4)$$

The parameters (V, α), the phase shift ϕ , and τ , the ratio between the periods of the 1D lattice and the QP modulation, fully characterize the potential. We take τ to be the inverse of the Golden Ratio, $\tau = \varphi_R^{-1} = (\sqrt{5} - 1)/2$. For reducing finite-size effects, we consider rational approximants given by the ratio of two successive Fibonacci numbers, $\tau_j = F_{j-1}/F_j$, with $\tau = \tau_\infty$, and take $L = F_j$. We

also average the numerical results over random boundary twists, θ , and shifts, ϕ , to further reduce finite-size effects.

For the AA model, transitions between delocalized ($0 < V < 2t$) and localized ($V > 2t$) states are energy independent and occur at $V_c = 2t$, as shown in Fig. 1(a). For the GPS model, the mobility edge is given by $E = (V \pm 2t)/\alpha$ [8], while the critical region is delimited by $|V - E\alpha| \leq |2t\alpha| \wedge |\alpha| \geq 1$ [7], as seen in Fig. 1(c).

In order to characterize phase transitions and analyze localization properties of the wavefunctions, we use the inverse participation ratio (IPR):

$$\text{IPR}[\psi] = \sum_n |\psi_n|^4, \quad (5)$$

where ψ is the normalized fermionic wavefunction. The IPR shows a power law scaling, $\text{IPR}[\psi] \sim L^{-\tau_F}$, with $\tau_F = 0$ for localized states, $\tau_F = d$ for extended states (d is the dimension) and $\tau_F = D_F$ for multifractal states (D_F is the fractal dimension, obeying $0 < D_F < d$) [7, 47, 48]. The scaling analysis of the τ_F exponent shows that, for fermionic systems, the IPR of both extended and multifractal states tends to zero in the thermodynamic limit. Conversely, localization in momentum space can be quantified by the momentum space IPR (IPR_κ) [49]:

$$\text{IPR}_\kappa[\psi] = \sum_k |\tilde{\psi}_k|^4, \quad (6)$$

where $\tilde{\psi}_k$ are the Fourier coefficients of the wave function. $\text{IPR}_\kappa[\psi] \sim L^{-\tau_F^\kappa}$, with $\tau_F^\kappa = d$ for localized and $\tau_F^\kappa = 0$ for ballistic states. At criticality, both IPR and the IPR_κ decrease with L . For studying localization properties of the bosonic systems, we consider $\text{IPR}[\Phi^n]$ and the $\text{IPR}_\kappa[\Phi^n]$, with Φ^n the n -th NO.

Results. — Consider the AA model defined by Eq. (1) with the on-site potential in Eq. (3). For completeness, we show the single-particle results in Fig. 1(a), where the well-known energy-independent localization transition at $V_c = 2$ is clearly seen in the IPR values. Figure 1(b) depicts the scaling of λ_0 with the system size at filling fraction ($\nu = N_b/L$) $\nu = 1/2$, for different values of V . For $V < V_c$ ($V > V_c$), the scaling $\lambda_0 \propto L^\gamma$ with $\gamma = 1/2$ ($\gamma = 0$) is recovered for the quasicondensed (Bose glass) state. At criticality ($V = V_c$), the AA model behaves as a Bose superfluid. For $\nu = 1/2$ (blue curve), the exponent $\gamma \simeq 0.25 \pm 0.01$ is obtained. quasicondensation still occurs for $\nu \neq 1/2$, albeit with a smaller value for γ . The green curve in Fig. 1(b) shows the results at criticality for $\nu = 0.29$, where the corresponding scaling exponent is given by $\gamma \simeq 0.16 \pm 0.01$.

Now we turn to the GPS model, given by Eq. (1) with the incommensurate potential of Eq. (4). Figure 1(c)

shows the density plot of the single-particle IPR as a function of the energy and of the parameter α . For $\alpha < 1$, only extended-localized transitions are observed. Transitions between critical-extended and critical-localized states occur at $\alpha = 1$ and $\alpha > 1$, respectively.

Figure 1(d) shows the scaling of λ_0 , for two values of the parameters (α, ν) in the critical region indicated in Fig. 1(c). As for the AA model, we find $0 < \gamma < 1/2$, indicating the presence of an exotic quasicondensed state. Specifically, we obtain $\gamma = 0.27 \pm 0.01$ and $\gamma = 0.33 \pm 0.01$ for $(\alpha, \nu) = (2, 0.48)$ and $(\alpha, \nu) = (3.5, 0.368)$, respectively. We attribute the different scaling exponents to the parameter-dependent fractal properties of the single-particle states [47, 50, 51] which manifest in the bosonic NO through an exotic type of quasicondensation, here dubbed fractal quasicondensation, with a tunable scaling exponent γ . It should be noted that even for a model without energy-dependent mobility edges, such as the AA model, such scaling exponent can be tuned by means of the filling fraction.

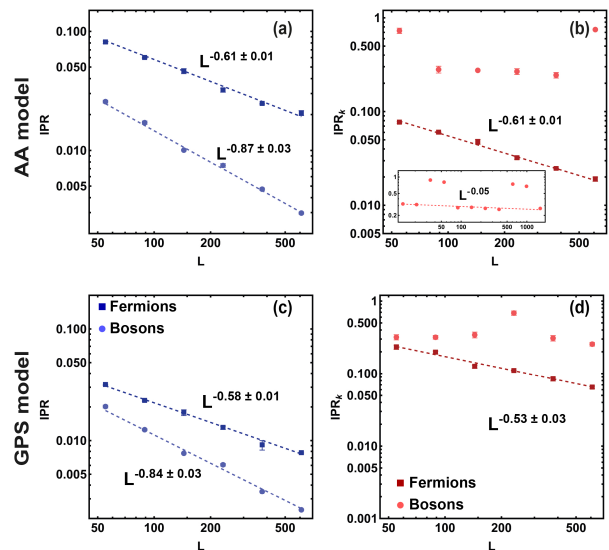


FIG. 2. **AA model** ($V = 2$). (a) IPR scaling of the fermionic eigenvectors (natural orbitals), indicated by dark (light) blue points with error bars, where the dark (light) red curve corresponds to the fitted model $\text{IPR} \sim L^{-\tau_{F,B}}$, with the exponent $\tau_F = 0.61 \pm 0.01$ ($\tau_B = 0.87 \pm 0.03$). (b) IPR_κ scaling of the fermionic eigenvectors (natural orbitals), indicated by dark (light) red points. The IPR_κ of the fermionic eigenvectors scales as $\text{IPR}_\kappa \sim L^{-\tau_F^\kappa}$, with $\tau_F^\kappa = 0.61 \pm 0.01$. Inset shows the scaling of the NO's IPR_κ for larger system sizes, up to $L = 1597$. **GPS model** ($V = 0.75$, $\alpha = 3.5$, $\nu = 0.368$). (c) IPR scaling of the fermionic eigenvectors (natural orbitals), indicated by dark (light) blue points, where the dark (light) curve is a fit yielding the the exponent $\tau_F = 058 \pm 0.01$ ($\tau_B = 0.84 \pm 0.03$). (d) IPR_κ scaling of the fermionic eigenvectors (natural orbitals), indicated by dark (light) red points, with $\tau_F = 0.53 \pm 0.03$ for the fermionic eigenvectors.

To investigate the fractal nature of the natural orbitals at criticality, we compute the scaling of their IPR and

IPR $_{\kappa}$, as defined by Eqs. (5) and (6), respectively. The results are compared with the scalings of the single-particle eigenstates at the same filling. This analysis is made for the AA model at $V = 2$ in Fig. 2(a,b), and for the GPS model in Fig. 2(c,d).

The IPR of the NO in Fig. 2(a) scales as $\text{IPR}[\Phi] \sim L^{-\tau_B}$ with a scaling exponent $0 < \tau_B < 1$, indicating multifractality, albeit with an exponent larger than its fermionic counterpart, i.e. $\tau_B > \tau_F$. The results for the fermionic, $\text{IPR}_{\kappa}[\psi] \sim L^{-\tau_F}$, and bosonic, $\text{IPR}_{\kappa}[\psi] \sim L^{-\tau_B}$, scalings of the IPR $_{\kappa}$ in Fig. 2(b) are, however, considerably different. As shown in the inset of Fig. 2(b), the IPR $_{\kappa}$ of NO remains essentially constant, decreasing very slowly as $L^{-0.05}$, with unexpected fluctuations at $L = \{34, 55, 610, 987\}$. Also, the scaling exponent of the bosonic IPR, τ_B , is closer to 1 than in the fermionic case. These observations for $V = 2$ could lead to the erroneous conclusion that the localization-delocalization transition for the bosonic NO occurs for a critical potential $V_c > 2$. As we argue below, the transition still occurs at $V_c = 2$ as in the fermionic case, if finite-size effects are carefully taken into account.

Similar results were found for the GPS model. The IPR and IPR $_{\kappa}$ of the fermionic eigenvectors (natural orbitals) for $\nu = 0.368$ are shown in Figs. 2(c,d). The IPR $_{\kappa}$ of the natural orbitals for the GPS model also slowly decreases with L , as seen in Fig. 2(d). The results of the GPS model with $\nu = 0.48$ show similar qualitative behavior, with different values for $\tau_{F,B}$, due to the fractality of the eigenstates (see Sec. (S1) of Supplemental Material).

To understand the atypical behavior of the NO's IPR $_{\kappa}$, we turn once again to the AA model. Figure 3 displays the IPR (IPR $_{\kappa}$) of the NO as a function of the potential V , for different system sizes. For small (high) V , the IPR (IPR $_{\kappa}$) of the NO decreases with L . For high (small) V , the IPR (IPR $_{\kappa}$) becomes L -independent. All these behaviors are similar to those of the fermionic eigenvectors. The main difference occurs for intermediate $V \gtrsim 2$, when $V \rightarrow 2$ from above: in such regime, the IPR $_{\kappa}$ does not scale down with L , as it would be expected for localized NOs. However, Fig. 3 suggests that this is a finite-size effect, as can be inferred from the drift of the $\text{IPR} = \text{IPR}_{\kappa}$ crossing point towards $V = 2$ with increasing size. These results substantiate our hypothesis that the localization transition for the NO occurs at $V_c = 2$, as in the fermionic case. Nevertheless, in contrast to the latter, the localization length in the localized phase may be larger for NOs, even for V significantly larger than 2. The inset in Fig. 3 corroborates the multifractal nature of the NOs, showing that the crossing point between the IPR and the IPR $_{\kappa}$ decreases with system size as $\sim L^{-0.47}$.

Discussion. — In this letter, we studied the condensation of HCB in the presence of quasiperiodic-induced critical states with multifractal wavefunctions with the help of the Jordan-Wigner mapping to non-interacting fermions. We show that when the chemical potential

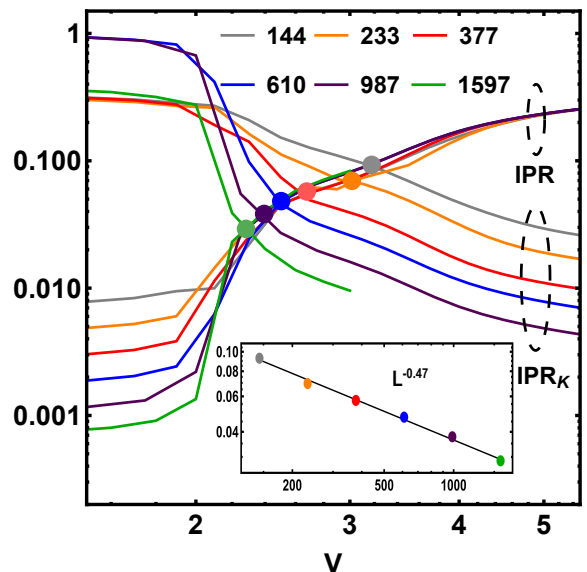


FIG. 3. **AA Model.** IPR and IPR $_{\kappa}$ of the NOs versus the on-site potential (V) for $L = 144, 233, 377, 610, 987, 1597$. As in the fermionic case, for small (high) potentials, the IPR (IPR $_{\kappa}$) of the natural orbitals decreases with L . For high (small) potentials, the IPR (IPR $_{\kappa}$) does not change with system size. For $V \gtrsim 2$, the large L scaling behavior is less clear. However, the value of the on-site potential for which $\text{IPR} = \text{IPR}_{\kappa}$ gets closer to $V = 2$ as L increases, which indicates the presence of important finite-size effects on the NOs analysis. The inset shows the scaling of the crossing point between NO's IPR and IPR $_{\kappa}$, revealing its multifractal behavior.

is placed in regions of critical states, quasicondensation acquires exotic features. This regime, we dubbed fractal quasicondensation, is characterized by the growth of the occupation of the lowest natural orbital, albeit with an exponent smaller than the value, $\nu = 1/2$, observed in one-dimension quasicondensates with ballistic single-particle states.

This mechanism of quasicondensation can be probed in state-of-the-art experiments with cold atomic gases. Although implementing the QP potential described in Eq. (4) may be challenging, a simplified version of the model that still possesses a critical phase region is feasible (see (S2)). This simplified model is physically realizable with conventional optical lattice techniques, as shown by Liu et al. [7] for the fermionic case. As in previous works, the HCB constraint can be guaranteed by tuning the Feshbach resonances to make the interaction strength much higher than any other energy scale involved [52–58].

-
- [1] P. W. Anderson, Physical review **109**, 1492 (1958).
 - [2] S. Aubry and G. André, Ann. Israel Phys. Soc **3**, 18 (1980).
 - [3] E. Abrahams, P. W. Anderson, D. C. Licciardello, and

- T. V. Ramakrishnan, *Phys. Rev. Lett.* **42**, 673 (1979).
- [4] A. MacKinnon and B. Kramer, *Phys. Rev. Lett.* **47**, 1546 (1981).
- [5] P. A. Lee and T. Ramakrishnan, *Reviews of Modern Physics* **57**, 287 (1985).
- [6] M. Continentino, *Quantum scaling in many-body systems* (Cambridge University Press, 2017).
- [7] T. Liu, X. Xia, S. Longhi, and L. Sanchez-Palencia, *SciPost Physics* **12**, 027 (2022).
- [8] S. Ganeshan, J. Pixley, and S. D. Sarma, *Physical review letters* **114**, 146601 (2015).
- [9] M. Gonçalves, B. Amorim, E. Castro, and P. Ribeiro, *SciPost Physics* **13**, 046 (2022), 2103.03895.
- [10] M. Gonçalves, B. Amorim, E. V. Castro, and P. Ribeiro, *Physical Review B* **108**, L100201 (2023), arXiv:2206.13549.
- [11] M. Gonçalves, P. Ribeiro, E. V. Castro, and M. A. Araújo, *Physical Review Letters* **124**, 136405 (2020).
- [12] P. Ribeiro, M. Haque, and A. Lazarides, *Physical Review A* **87**, 043635 (2013).
- [13] Y. Wang, X. Xia, L. Zhang, H. Yao, S. Chen, J. You, Q. Zhou, and X.-J. Liu, *Physical Review Letters* **125**, 196604 (2020).
- [14] J. Biddle, D. Priour Jr, B. Wang, and S. D. Sarma, *Physical Review B* **83**, 075105 (2011).
- [15] X. Deng, S. Ray, S. Sinha, G. Shlyapnikov, and L. Santos, *Physical review letters* **123**, 025301 (2019).
- [16] M. Gonçalves, B. Amorim, E. V. Castro, and P. Ribeiro, (2022), 10.48550/arxiv.2208.07886, arXiv:2208.07886.
- [17] Y. Lahini, R. Pugatch, F. Pozzi, M. Sorel, R. Morandotti, N. Davidson, and Y. Silberberg, *Physical review letters* **103**, 013901 (2009).
- [18] D. Tanese, E. Gurevich, F. Baboux, T. Jacqmin, A. Lemaître, E. Galopin, I. Sagnes, A. Amo, J. Bloch, and E. Akkermans, *Physical review letters* **112**, 146404 (2014).
- [19] K. Singh, K. Saha, S. A. Parameswaran, and D. M. Weld, *Physical Review A* **92**, 063426 (2015).
- [20] T. Kohler, S. Scherg, X. Li, H. P. Lüschen, S. D. Sarma, I. Bloch, and M. Aidelsburger, *Physical review letters* **122**, 170403 (2019).
- [21] H. Yao, H. Khoudli, L. Bresque, and L. Sanchez-Palencia, *Physical review letters* **123**, 070405 (2019).
- [22] F. A. An, K. Padavić, E. J. Meier, S. Hegde, S. Ganeshan, J. H. Pixley, S. Vishveshwara, and B. Gadway, *Physical Review Letters* **126**, 040603 (2021).
- [23] M. Gonçalves, H. Z. Olyaei, B. Amorim, R. Mondaini, P. Ribeiro, and E. V. Castro, *2D Materials* **9**, 011001 (2022), arXiv:2008.07542.
- [24] J. H. Wilson, Y. Fu, S. D. Sarma, and J. Pixley, *Physical Review Research* **2**, 023325 (2020).
- [25] D. Vu and S. D. Sarma, *Physical Review Letters* **126**, 036803 (2021).
- [26] M. Gonçalves, B. Amorim, F. Riche, E. V. Castro, and P. Ribeiro, (2023), arXiv:2305.03800.
- [27] M. Gonçalves, J. H. Pixley, B. Amorim, E. V. Castro, and P. Ribeiro, (2023), arXiv:2304.09197.
- [28] Y. Cao, V. Fatemi, A. Demir, S. Fang, S. L. Tomarken, J. Y. Luo, J. D. Sanchez-Yamagishi, K. Watanabe, T. Taniguchi, E. Kaxiras, *et al.*, *Nature* **556**, 80 (2018).
- [29] Y. Cao, V. Fatemi, S. Fang, K. Watanabe, T. Taniguchi, E. Kaxiras, and P. Jarillo-Herrero, *Nature* **556**, 43 (2018).
- [30] L. Sanchez-Palencia and L. Santos, *Physical Review A* **72**, 053607 (2005).
- [31] Y. Eksioğlu, P. Vignolo, and M. Tosi, *Optics communications* **243**, 175 (2004).
- [32] G. Roati, C. DErrico, L. Fallani, M. Fattori, C. Fort, M. Zaccanti, G. Modugno, M. Modugno, and M. Inguscio, *Nature* **453**, 895 (2008).
- [33] M. Modugno, *New Journal of Physics* **11**, 033023 (2009).
- [34] M. A. Rigol and A. Muramatsu, *Journal of low temperature physics* **138**, 645 (2005).
- [35] H. Yao, T. Giamarchi, and L. Sanchez-Palencia, *Physical Review Letters* **125**, 060401 (2020).
- [36] S. Lellouch and L. Sanchez-Palencia, *Physical Review A* **90**, 061602 (2014).
- [37] B. Damski, J. Zakrzewski, L. Santos, P. Zoller, and M. Lewenstein, *Physical review letters* **91**, 080403 (2003).
- [38] C. DErrico, E. Lucioni, L. Tanzi, L. Gori, G. Roux, I. P. McCulloch, T. Giamarchi, M. Inguscio, and G. Modugno, *Physical review letters* **113**, 095301 (2014).
- [39] R. Roth and K. Burnett, *Physical Review A* **68**, 023604 (2003).
- [40] L. Fallani, J. Lye, V. Guarrera, C. Fort, and M. Inguscio, *Physical review letters* **98**, 130404 (2007).
- [41] M. Rigol and A. Muramatsu, *Physical Review A* **70**, 031603 (2004).
- [42] Y. Wang, C. Cheng, X.-J. Liu, and D. Yu, *Physical Review Letters* **126**, 080602 (2021).
- [43] F. A. An, K. Padavić, E. J. Meier, S. Hegde, S. Ganeshan, J. Pixley, S. Vishveshwara, and B. Gadway, *Physical review letters* **126**, 040603 (2021).
- [44] F. Riche, M. Gonçalves, B. Amorim, E. Castro, and P. Ribeiro, *Supplemental Material for Fractal Quasi-condensation in One-dimension*.
- [45] O. Penrose and L. Onsager, *Physical Review* **104**, 576 (1956).
- [46] A. J. Leggett, *Reviews of Modern Physics* **73**, 307 (2001).
- [47] A. Szabó and U. Schneider, *Physical Review B* **98**, 134201 (2018).
- [48] Y. Fu, E. J. König, J. H. Wilson, Y.-Z. Chou, and J. H. Pixley, *npj Quantum Materials* **5**, 1 (2020).
- [49] J. Pixley, J. H. Wilson, D. A. Huse, and S. Gopalakrishnan, *Physical review letters* **120**, 207604 (2018).
- [50] C. Tang and M. Kohmoto, *Phys. Rev. B* **34**, 2041 (1986).
- [51] H. Hiramoto and M. Kohmoto, *Phys. Rev. B* **40**, 8225 (1989).
- [52] M. Greiner, O. Mandel, T. Esslinger, T. W. Hänsch, and I. Bloch, *nature* **415**, 39 (2002).
- [53] C. Chin, R. Grimm, P. Julienne, and E. Tiesinga, *Reviews of Modern Physics* **82**, 1225 (2010).
- [54] S. Will, *From Atom Optics to Quantum Simulation: Interacting Bosons and Fermions in Three-Dimensional Optical Lattice Potentials* (Springer Science & Business Media, 2012).
- [55] T. Wasak, M. Krych, Z. Idziaszek, M. Trippenbach, Y. Avishai, and Y. Band, *Physical Review A* **90**, 052719 (2014).
- [56] M. Schreiber, S. S. Hodgman, P. Bordia, H. P. Lüschen, M. H. Fischer, R. Vosk, E. Altman, U. Schneider, and I. Bloch, *Science* **349**, 842 (2015).
- [57] S. Ray, M. Pandey, A. Ghosh, and S. Sinha, *New Journal of Physics* **18**, 013013 (2015).
- [58] T.-S. Deng, W. Zhang, and W. Yi, *Physical Review A* **96**, 050701 (2017).
- [59] S. Fishman, D. Grempel, and R. Prange, *Physical Review Letters* **49**, 509 (1982).

- [60] D. Grempel, R. Prange, and S. Fishman, *Physical Review A* **29**, 1639 (1984).
- [61] S. Longhi, *Optics Letters* **46**, 637 (2021).

Supplemental Material: Fractal quasicondensation in One-dimensional Systems

In this supplemental material we provide additional details of our analysis and some extra numerical calculations. The results are organized as follows: Sec. S1 analyzes the IPR scalings of fermionic and bosonic eigenvectors for another phase-space state of the GPS model at criticality and Sec. (S2) describes how to overcome challenges related with the implementation of unbounded potentials by resorting to Floquet engineered Hamiltonians.

S1. ADDITIONAL RESULTS FOR THE GPS MODEL AT CRITICALITY

For completeness, we also show the results of the IPR scalings for the fermionic vectors and for the natural orbitals of another phase-space state of the GPS model, with $V = 0.75$, $\alpha = 2$, $\nu = 0.48$. The results are similar to those obtained in the main article, depicted in Figs. 2(c,d). As we can see in Fig. S1, the scaling exponent of the fermionic eigenvectors is less than one for the IPR both in position and in momentum space. For the natural orbitals, due to the finite-size effects discussed in the main text, it was only possible to determine the scaling exponent of the IPR in position space, which was also less than one, as expected for fractal states.

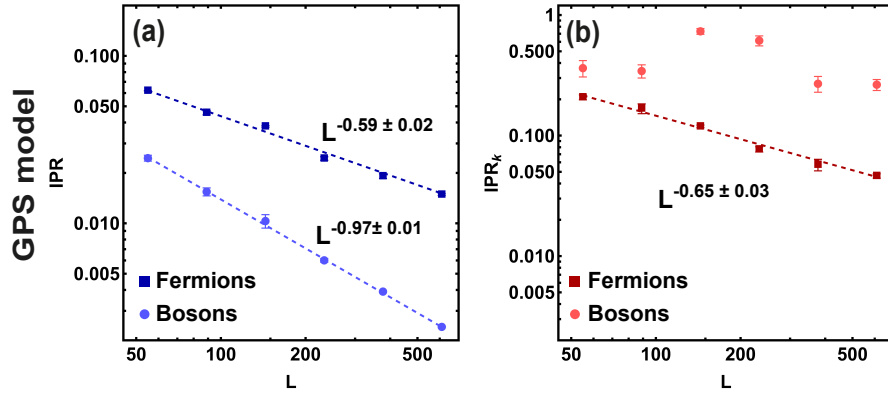


FIG. S1. IPR and IPR_k analysis inside the critical phase of the GPS model ($V = 0.75$, $\alpha = 2$, $\nu = 0.48$). (a) IPR scaling of the fermionic eigenvectors (natural orbitals), indicated by dark (light) blue points, where the dark (light) curve corresponds to the fitting, with the exponent $\tau_F = 0.59 \pm 0.02$ ($\tau_B = 0.97 \pm 0.01$). (b) IPR_k scaling of the fermionic eigenvectors (natural orbitals), indicated by dark (light) red points. The IPR_k of the fermionic eigenvectors scales as $\tau_F = 0.65 \pm 0.03$. The results were averaged over 10 random configurations of twists θ and phases ϕ .

S2. FLOQUET ENGINEERED HAMILTONIANS AND THE IMPLEMENTATION OF UNBOUNDED POTENTIALS

We now discuss in more details how to overcome problems related with the physical implementation of the GPS model in order to probe fractal quasicondensation. The unbounded potential described by Eq. (4) may show divergences leading to large arbitrary energies for $\alpha \geq 1$, due to phase fluctuations. To overcome this obstacle we can resort to a *Floquet Engineered Hamiltonian* [59–61]. Here we show how to map the Floquet eigenvalue equation onto the following tight-binding equation:

$$H = -t \sum_x (c_x^\dagger c_{x+1} + \text{h.c.}) + \sum_x \frac{V}{1 + \alpha \cos(2\pi\tau x_x + \phi)} c_x^\dagger c_x. \quad (\text{S1})$$

Since the difficulties of the implementation of the GPS model are associated only with the denominator of Eq. (4), our approach simplifies the problem, making the calculations more straightforward. In fact, the model depicted by Eq. (S1) also possesses a critical phase region where quasicondensation can be probed. Figure S2(a) shows the density

plot of the IPR as a function of the single-particle energy and of the on-site potential, with $\tau = 377/610$, and system size $L = 610$. Figure S2(b) depicts the scaling of the NO's eigenvalue (λ_0) with the system size for $(\nu, \alpha) = (0.49, 2.75)$, where the quasicondensation behavior is revealed by the sub-linear scaling ($L^{0.19 \pm 0.02}$).

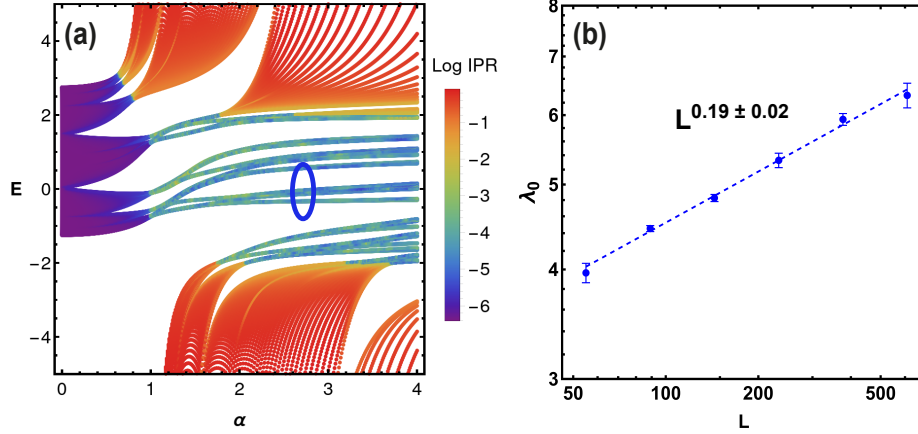


FIG. S2. (a) Density plot of the IPR as a function of the energy and of the on-site potential, for $L = 610$. (b) Scaling of the natural orbital's highest eigenvalue (λ_0) at the critical point, for $(\nu, \alpha) = (0.49, 2.75)$ (blue points). The quasicondensation behavior is revealed by the sub-linear scaling ($L^{0.19 \pm 0.02}$), where L is the system size. The results were averaged over 10 random configurations of twists θ and phases ϕ .

Following the approach of Ref. [7] we start from a periodically-kicked quantum 1D system, described by the Schrödinger equation (in units where $\hbar = 1$):

$$K(p) \sum_n \delta(t - nT) |X, t\rangle + V(x) |X, t\rangle = i \partial_t |X, t\rangle. \quad (\text{S2})$$

The advantage of kicking the kinetic term, instead of the more common approach where the potential term is periodically kicked, is that we can recover Eq. S1 in position space, which is relevant in our case due to the role of interactions in Bose superfluidity. The evolution of the wavefunction for one kick is given by:

$$e^{-i \sum_x V_x c_x^\dagger c_x} e^{-i \sum_p K_p c_p^\dagger c_p} |x, t = m\rangle = |x, t = m + 1\rangle, \quad (\text{S3})$$

where $V(x) = \sum_x V_x c_x^\dagger c_x$ and $K(p) = \sum_p K_p c_p^\dagger c_p$. By defining $|X, t = m\rangle \equiv |X\rangle e^{-i\mu m}$, where $-\pi \leq \mu \leq \pi$ is the Floquet quasi-energy, we can rewrite Eq. (S3) in terms of a spectral problem:

$$e^{-i \sum_x V_x c_x^\dagger c_x} e^{-i \sum_p K_p c_p^\dagger c_p} |X\rangle = e^{-i\mu} |X\rangle. \quad (\text{S4})$$

The next step is to introduce the auxiliary operator, $W(p) \equiv \tan\left(\frac{\sum_p K_p c_p^\dagger c_p}{2}\right)$, which gives:

$$e^{-i \sum_p K_p c_p^\dagger c_p} = \frac{1 - iW(p)}{1 + iW(p)}. \quad (\text{S5})$$

We also define:

$$|X\rangle \equiv [1 + iW(p)]|x\rangle. \quad (\text{S6})$$

Eqs. (S5) and (S6) in Eq. (S4) yields:

$$[1 + iW(p)]|x\rangle = e^{i\mu - i \sum_x V_x c_x^\dagger c_x} [1 - iW(p)]|x\rangle, \quad (\text{S7})$$

which can be rewritten as:

$$W(p)|x\rangle = S_x|x\rangle, \quad (\text{S8})$$

where $\frac{1+iS_x}{1-iS_x} = e^{i\mu-i\sum_x V_x c_x^\dagger c_x}$. Also:

$$W(p) = \sum_p W_p c_p^\dagger c_p |p\rangle\langle p| = \sum_{x,x'} |x\rangle W_{x-x'} \langle x'|, \quad (\text{S9})$$

and from Eq. (S9) in (S8):

$$\sum_{x,x'} |x\rangle W_{x-x'} \langle x'|x\rangle = S_x|x\rangle. \quad (\text{S10})$$

Now we show how to recover the tight-binding model of Eq. (S1), starting from the left-hand side of Eq. (S10), from which we are going to derive the hopping terms. Since $K(p) = \sum_p K_p c_p^\dagger c_p$ is diagonal in Bloch basis, with energies $\varepsilon_p = -2t \cos(p)$, we can write the auxiliary operator as:

$$W(p) = \tan\left(\frac{\varepsilon_p}{2}\right) \sim \frac{\varepsilon_p}{2} = -t \cos(p), \quad (\text{S11})$$

since the kick time is much smaller than the inter-kick time, $\tau \ll T$. Considering only first neighbors, Eq. (S10) reads:

$$-t|x-1\rangle - t|x+1\rangle = S_x|x\rangle. \quad (\text{S12})$$

The right-hand side of Eq. (S8) will give us the QP potential and the eigenvalues based on the Floquet quasi-energy. By defining $E \equiv 1/\tan(\mu/2)$ and rewriting $\frac{1+iS_x}{1-iS_x} = e^{i\mu-i\sum_x V_x c_x^\dagger c_x}$ we obtain

$$S_x = E - \sum_x \frac{V}{1 + \frac{1}{E} \tan\left(\frac{V_x}{2}\right)} c_x^\dagger c_x, \quad (\text{S13})$$

where $V \equiv \frac{1+E^2}{E}$.

To recover Eq. (S1) we set $V_x = 2 \arctan[A \cos(2\pi\tau x_n + \phi)]$. The QP potential in Eq. (S13) becomes:

$$\sum_x \frac{V}{1 + \alpha \cos(2\pi\tau x_n + \phi)} c_x^\dagger c_x, \quad (\text{S14})$$

where $\alpha = A/E$, varying without divergences.